arXiv:1403.6885v2 [cond-mat.mtrl-sci] 7 Apr 2014

Driving ferromagnets into a critical region of a magnetic phase diagram

B. Y. Mueller* and B. Rethfeld
Department of Physics and Research Center OPTIMAS, University of Kaiserslautern, Erwin-Schrödinger-Str. 46, 67653 Kaiserslautern, Germany
(Dated: April 9, 2014)

Exciting a ferromagnetic sample with an ultrashort laser pulse leads to a quenching of the magnetization on a subpicosecond timescale. On the basis of the equilibration of intensive thermodynamic variables we establish a powerful model to describe the demagnetization dynamics. We demonstrate that the magnetization dynamics is mainly driven by the equilibration of chemical potentials. The minimum of magnetization is revealed as a transient electronic equilibrium state. Our method identifies the slowing down of ultrafast magnetization dynamics by a critical region within a magnetic phase diagram.

PACS numbers: 75.78.-n, 75.78.Jp, 05.70.Ln

The strong increase of computational power within the last thirty years has also boosted the need for large and fast data storage. However, the physical speed limits of conventional magnetic recording, which are on the order of nanoseconds, are nowadays reached [1]. A promising enhancement lies in a subpicosecond change of magnetization, as has been found in 1996 by exciting a ferromagnetic material with an ultrashort laser pulse [2]. Though, a detailed understanding of the underlying physical processes of this ultrafast demagnetization is still lacking and several models compete, hampering the further development [3–6].

The most promising concepts are based on superdiffusive spin transport [7–10] or Elliott-Yafet (EY) spin-flip processes [5, 6, 11–21]. It has been shown experimentally, that both processes contribute to the magnetization dynamics, depending on the sample geometry [3, 9]. On the one hand, superdiffusive transport dominates on bulk and multilayer systems and has been successfully compared to experiments [8, 9]. On the other hand, EY spin-flip scattering has been investigated with kinetic models and reproduces the magnetization dynamics for thin films [14–16]. Due to the complexity of the methods, temperature-based models have been proposed, like the microscopic three temperature model (M3TM) [12, 21]. Recently, it has been shown, that this simplification is justified, despite of an ultrafast laser excitation [14].

In this Letter, we derive a μT model (μTM), which traces the dynamics and the equilibration of temperatures and chemical potentials of the electron subsystems simultaneously. The essential concepts of the μTM are based on a kinetic approach [13–15], including EY-type spin-flip scattering and a dynamic exchange splitting [11, 14]. The μTM reproduces the experimental magnetization curves for different laser fluences. We find that the equilibration of chemical potentials drives the dynamics of the magnetization and the magnetization minimum is revealed as a transient equilibrium state within a magnetic phase diagram. We identify a critical region within this phase diagram: For certain fluences, the material is driven into this region, causing an extreme deceleration of the magnetization dynamics. This finding confirms the experimental observation of a critical slowing down [12, 21]. Unlike the M3TM, we trace the dynamics of minority and majority electron densities explicitly, which opens the possibility to extend the model for superdiffusive transport effects.

A general matrix formulation of a time- and space-dependent coupled transport equation is given by

$$C\frac{d}{dt}\vec{X} = \nabla K \nabla \vec{X} + G\vec{X} + \vec{S} \ , \tag{1}$$

where $\vec{X}$ is the vector of transient variables, C, K and G are matrices of capacities, transport and coupling, respectively, and $\vec{S}$ is the source vector. A representative of such equation system is the well-known two temperature model (TTM) [22] of two coupled heat conduction equations. In that case the vector of interest $\vec{X}$ consists of the respective electron and lattice temperature, T_e and T_ℓ, the source vector contributes to the equation for the electron energy, and the capacity matrix as well as the transport matrix are diagonal matrices. The temperatures are coupled through an equilibration term, $\pm g\,(T_e - T_\ell)$, thus the coupling matrix G contains also off-diagonal elements. Here, g is the electron–lattice coupling parameter.

In itinerant ferromagnets, the electrons of majority and minority spins can be treated separately. The temperatures of both electron types, denoted by $T_e^\uparrow$ and $T_e^\downarrow$, respectively, may differ. Moreover, the respective particle densities may change due to EY spin-flip processes and only their sum $n = n^\uparrow + n^\downarrow$ is constant. Therefore, the chemical potentials $\mu^\uparrow$ and $\mu^\downarrow$ have to be considered as further variables of $\vec{X}$ in Eq. (1). Further, in the frame of an effective Stoner model [14, 23], the densities of states $D^\uparrow(E)$ and $D^\downarrow(E)$ of up- and down electrons, respectively, are shifted by an exchange splitting Δ. This exchange splitting is not constant but is directly coupled with the magnetization m through the effective Coulomb interaction U [23]. In Ref. 14 it was shown that the in-

stantaneous feedback of the transient magnetization on the exchange splitting,

$$\Delta(t) = Um(t) \ , \tag{2}$$

is essential for the quantitative description of demagnetization dynamics. The normalized magnetization $m(t)$ results from the transient particle density of each electron reservoir as

$$m(t) = \left(n^{\uparrow}(t) - n^{\downarrow}(t)\right)/n \ . \tag{3}$$

The particle density $n^{\sigma}\left(T_e^{\sigma}, \mu^{\sigma}, m\right)$ and internal energy density $u_e^{\sigma}\left(T_e^{\sigma}, \mu^{\sigma}, m\right)$ of the spin $\sigma \in \{\uparrow, \downarrow\}$ are calculated by the zeroth and first moment of the current Fermi distribution $f\left(E, T_e^{\sigma}, \mu^{\sigma}\right)$. Thus, under the given conditions both, particle density and internal energy density, depend on the two intrinsic variables T_e^{σ} and μ^{σ} and on the magnetization which determines the energy shift of the exchange splitting Δ, see Eq. (2). The temporal derivatives of the energy density u_e^{σ} and the particle density n^{σ} include partial derivatives, e.g.

$$\frac{du_e^{\sigma}}{dt} = c_T^{\sigma}\frac{\partial T_e^{\sigma}}{\partial t} + c_{\mu}^{\sigma}\frac{\partial \mu^{\sigma}}{\partial t} + c_m^{\sigma}\frac{\partial m}{\partial t} \ , \tag{4}$$

defining the capacity equivalents $c_x^{\sigma} \equiv \frac{\partial u_e^{\sigma}}{\partial x}$. Analogously, partial derivatives of the particle density are defined as $p_x^{\sigma} \equiv \frac{\partial n^{\sigma}}{\partial x}$. This allows us to mathematically separate the variables T_e^{σ}, μ^{σ} and m.

To demonstrate the power of the μT model and to separate the time-dependent effects from transport effects, we restrict ourselves here to the temporal dependence of the decisive variables, which is capable to predict and explain important characteristics of the magnetization dynamics of thin ferromagnetic films. The temporal evolution of $T_e^{\uparrow}, T_e^{\downarrow}, T_{\ell}, \mu^{\uparrow}, \mu^{\downarrow}$ and m is expressed with an equation of type (1):

$$\begin{pmatrix} c_T^{\uparrow} & 0 & 0 & c_{\mu}^{\uparrow} & 0 & c_m^{\uparrow} \\ 0 & c_T^{\downarrow} & 0 & 0 & c_{\mu}^{\downarrow} & c_m^{\downarrow} \\ 0 & 0 & c_{\ell} & 0 & 0 & 0 \\ p_T^{\uparrow} & 0 & 0 & p_{\mu}^{\uparrow} & 0 & p_m^{\uparrow} \\ 0 & p_T^{\downarrow} & 0 & 0 & p_{\mu}^{\downarrow} & p_m^{\downarrow} \\ -p_T^{\uparrow} & p_T^{\downarrow} & 0 & -p_{\mu}^{\uparrow} & p_{\mu}^{\downarrow} & n^{\uparrow}+n^{\downarrow} \end{pmatrix} \frac{d}{dt} \begin{pmatrix} T_e^{\uparrow} \\ T_e^{\downarrow} \\ T_{\ell} \\ \mu^{\uparrow} \\ \mu^{\downarrow} \\ m \end{pmatrix} = \begin{pmatrix} -\gamma-g^{\uparrow} & \gamma & g^{\uparrow} & 0 & 0 & 0 \\ \gamma & -\gamma-g^{\downarrow} & g^{\downarrow} & 0 & 0 & 0 \\ g^{\uparrow} & g^{\downarrow} & -g^{\uparrow}-g^{\downarrow} & 0 & 0 & 0 \\ 0 & 0 & 0 & -\nu & \nu & 0 \\ 0 & 0 & 0 & \nu & -\nu & 0 \\ 0 & 0 & 0 & 0 & 0 & 0 \end{pmatrix} \begin{pmatrix} T_e^{\uparrow} \\ T_e^{\downarrow} \\ T_{\ell} \\ \mu^{\uparrow} \\ \mu^{\downarrow} \\ m \end{pmatrix} + \begin{pmatrix} S^{\uparrow}(t) \\ S^{\downarrow}(t) \\ 0 \\ 0 \\ 0 \\ 0 \end{pmatrix} . \tag{5}$$

The first three equations determine the energy of spin-up and spin-down electrons as well as of the lattice, respectively. Equations four and five trace the densities of both electron systems. The last equation defines the transient magnetization, Eq. (3). In the spirit of the TTM [22], we introduce an respective equilibration term for the electron temperatures, $\pm\gamma\left(T_e^{\uparrow} - T_e^{\downarrow}\right)$, and chemical potentials, $\pm\nu(\mu^{\uparrow} - \mu^{\downarrow})$. The laser excitation of each electron system is described by the source term $S^{\sigma}(t)$. To conserve the total energy with a dynamic exchange splitting, the correlation energy [23] $u_{\mathrm{Corr}}(t) = -Un^{\uparrow}(t)n^{\downarrow}(t)/n$ is taken into account in $c_T^{\uparrow,\downarrow}$, $c_{\mu}^{\uparrow,\downarrow}$ and $c_m^{\uparrow,\downarrow}$.

We solve the μTM for nickel, with the density of states from Ref. 24. The effective Coulomb interaction $U = 5.04$ eV reproduces the experimental [25] equilibrium magnetization curve well [14]. The lattice heat capacity is taken as $c_{\ell} = 3.776 \times 10^6$ J/Km^3 [26]. For simplicity, we introduce the same electron-lattice coupling $g^{\sigma} = g/2 = 1 \times 10^{18}$ W/Km^3 [27] for both electron systems. The coupling parameters between chemical potentials, $\nu = 5.80 \times 10^{60}$ 1/Jsm^3, and the inner-electronic temperature coupling, $\gamma = 163.8 \times g^{\sigma}$, are newly introduced in this work. They are determined through a fit of the transient magnetization curve obtained by the μTM to experimental data of Ref. 21. With the same laser parameters as in Ref. 21, and a reflectivity of $R = 0.44$, the μTM reproduces the magnetization curve for different fluences. A comparison between the experiment and the μT model is depicted in the upper panel of Fig. 1.

Figure 1 shows from top to bottom the dynamics of the magnetization, of the chemical potentials $\mu^{\uparrow}$ and $\mu^{\downarrow}$ and of the temperatures $T_e^{\uparrow}$, $T_e^{\downarrow}$ and T_{ℓ}. Two different fluences were applied for the calculations, $F_0 = 2.5$ mJ/cm^2 (blue curves) and $2 \times F_0$ (red curves). The minima of the magnetization curves are marked with vertical lines through all three panels of Fig. 1. The chemical potentials (central panel) of majority and minority electrons differ strongly during irradiation, equal each other for an instant cross-over and equilibrate on later timescales. The electron temperatures (lower panel) both grow fast during irradiation, however majority and minority temperatures differ due to the different heat capacities. After excitation, both electron temperatures equilibrate with each other and later also with the lattice temperature.

Inverting the capacity matrix C in Eq. (5) leads to a direct formulation for the temporal derivatives of $T_e^{\uparrow}, T_e^{\downarrow}, T_{\ell}, \mu^{\uparrow}, \mu^{\downarrow}$ and m. In particular, the change of magnetization is given by

$$\frac{dm}{dt} = -\frac{2\nu}{n}\left(\mu^{\uparrow} - \mu^{\downarrow}\right) \ , \tag{6}$$

where the time-dependence occurs only in the difference of the chemical potentials. Thus, the μTM directly identifies the equilibration of chemical potentials of majority and minority electrons as the driving force of magnetization dynamics, as proposed in Ref. 13.

Five characteristic points appear in the magnetization dynamics. They are indicated in the magnetization curve for the lower excitation in Fig. 1. Their origins are explained with the μT model in the following:

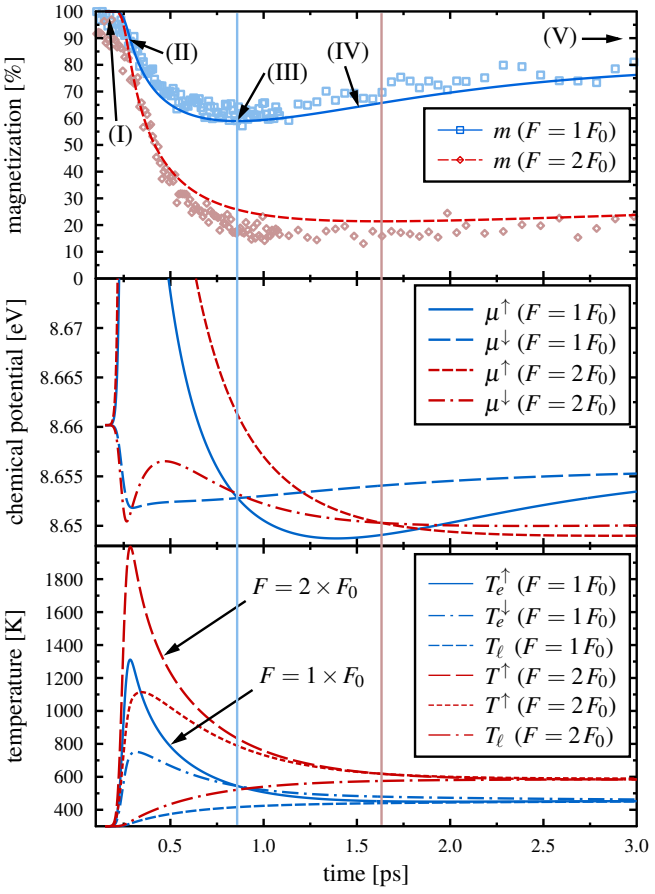

FIG. 1. Typical results of the μT model, transient magnetization (upper panel), chemical potentials (central panel) and temperatures (lower panel). The blue curves correspond to a low fluence $F_0 = 2.5\ \mathrm{mJ/cm^2}$, whereas the red curves are calculated after excitation with twice of that fluence, $2\times F_0$. In the upper panel, experimental results [21] are shown for comparison. The vertical lines indicate the respective time where the magnetization dynamics suffer a minimum. Characteristic points (I) to (V), as marked for the blue solid demagnetization curve, are analyzed in the text.

(I) We analyze the magnetization dynamics directly at the time when the laser hits the sample. Recent ab initio calculations did this as well [5, 6], concluding that the initial change of magnetization, $dm/dt|_{t=0}$, is too small to induce a reasonable demagnetization. This is in accordance with the μTM, that predicts even a vanishing first derivative, dm/dt, for the initial time step, when the chemical potentials are still in equilibrium $\mu^\uparrow = \mu^\downarrow$, see Eq. (6). The feedback effect, induced by a dynamic exchange splitting only occurs at later times, when the chemical potentials are driven out of equilibrium. The μTM explicitly accounts for the feedback effect and its influence can be illustrated by calculating the second derivative of Eq. (5) during a constant laser excitation

$$\frac{d^2m}{dt^2} = -\left(\frac{p_T^\uparrow}{c_\mu^\uparrow p_T^\uparrow - c_T^\uparrow p_\mu^\uparrow} - \frac{p_T^\downarrow}{c_\mu^\downarrow p_T^\downarrow - c_T^\downarrow p_\mu^\downarrow}\right)\frac{\nu S}{n}\ ,$$

assuming G and C as constant over the considered time interval. Initially, $d^2m/dt^2 \propto S(t=0)$ holds for very short times and the transient magnetization is determined mainly by $m(t) \approx m_0 + \frac{1}{2}\frac{d^2m}{dt^2}t^2$. Thus, even for vanishing $\frac{dm}{dt}|_{t=0}$ the description of demagnetization is possible by including a feedback effect, and ab initio calculations as in Ref. [4–6, 11] do not contradict the EY picture.

(II) After the excitation, the magnetization decreases rapidly, reaching the maximum change at the inflection point of the magnetization curve. Eq. (6) proposes, that also the nonequilibrium of chemical potentials is at its maximum, which is supported by Fig. 1.

(III) At the minimum of magnetization a transient equilibrium between the electron subsystems is observed. Here, the chemical potentials $\mu^\uparrow = \mu^\downarrow$ (as expected from Eq. (6)) and also the temperatures $T_e^\uparrow = T_e^\downarrow$ are equilibrated, both confirmed by Fig. 1. However, the lattice is still not in equilibrium with the electron system. In this transient equilibrium state, the μTM shows that the parabola approximation of the minimum,

$$\frac{d^2m}{dt^2} = \frac{2g\nu}{n}\left(\frac{p_T^\uparrow}{c_\mu^\uparrow p_T^\uparrow - c_T^\uparrow p_\mu^\uparrow} - \frac{p_T^\downarrow}{c_\mu^\downarrow p_T^\downarrow - c_T^\downarrow p_\mu^\downarrow}\right)(T_e - T_\ell)\,,$$

is mainly determined by the temperature difference between the electrons and the lattice.

(IV) After the transient equilibrium state of the electron subsystems, the chemical potentials are driven out of equilibrium again. This is due to the relaxation with the lattice. At the maximum difference between both chemical potentials, the second inflection point in the magnetization curve occurs.

(V) For larger times, the chemical potentials and temperatures of the electrons and the lattice equilibrate, see Fig. 1, and the magnetization reaches its equilibrium value $m\,(T_e)$.

The strength of the μTM is the possibility of analytical predictions about many relevant physical processes in ultrafast magnetization dynamics. In particular, we observe in Fig. 1 a so-called *critical slowing down* of magnetization dynamics [28, 29] for the high laser fluence. The reason is explained with Fig. 2, which depicts the phase diagram of m and T_e. For long excitations, in the order of nanoseconds, we expect that the magnetization follows the equilibrium magnetization $m\,(T_e)$ which is indicated as a black curve. However, the ultrashort laser pulse drives the system out of equilibrium and the magnetization becomes a function of $T_e^\uparrow, T_e^\downarrow, \mu^\uparrow$ and $\mu^\downarrow$. In particular, in these nonequilibrium states, the chemical potentials differ strongly, which is reflected in the central

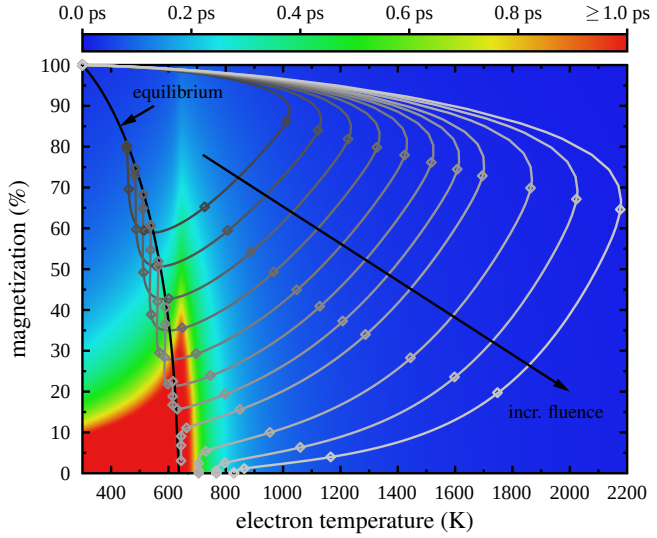

FIG. 2. Phase diagram of ultrafast magnetization dynamics. The black curve is the equilibrium magnetization cuve $m(T)$. The gray curves result from the μT model for the fluences $F/F_0 = 1.0, 1.2, ..., 2.4, 2.8, 3.2, 3.6$ with $F_0 = 2.5\,\mathrm{mJ/cm^2}$. The dots mark several times at $t = 0, 0.3, 0.5, 1, 2, 5, 10, 25$ ps. The background color labels the relaxation time towards the equilibrium magnetization.

panel of Fig. 1. The temperatures $T_e^{\uparrow}$ and $T_e^{\downarrow}$ are close to each other and are approximated by their mean value T_e for the following discussion. In Fig. 2, the parametric (m, T_e) curves of magnetization dynamics after different laser fluences are indicated by gray lines. All curves start at room temperature, top left of the diagram. Further dots up to 25 ps show the dynamical behavior on the parametric curves. The laser drives the system to high electronic temperatures, however, due to the nonequilibrium situation, the magnetization is still finite even for $T > T_C$. The first cross-over of the equilibrium magnetization curve, observed for fluences up to $2.2 \times F_0$, corresponds to the *transient equilibrium state* (III) and coincides with the minimum of the respective magnetization curve.

Importantly, the time to reach the final state on the equilibrium magnetization curve $m(T_e)$ differs for different fluences. For each pair (m, T_e) both chemical potentials $\mu^{\uparrow}, \mu^{\downarrow}$ can be determined by simultaneously solving Eq. (3) and the equation of particle conservation, $n = \text{const}$. We can estimate the time τ_{eq} to reach the equilibrium magnetization (black curve) for each point of m and T_e in the phase diagram by a relaxation time approximation of Eq. (6),

$$\frac{m\left(T_e, \mu^{\uparrow}, \mu^{\downarrow}\right) - m\left(T_e\right)}{\tau_{\mathrm{eq}}} = -\frac{2\nu}{n}\left(\mu^{\uparrow} - \mu^{\downarrow}\right) \quad . \qquad (7)$$

The relaxation time to equilibrium, τ_{eq}, is depicted in the background color code of Fig. 2. Under strong nonequilibrium conditions, especially at high temperatures, this relaxation occurs very fast: The large difference in chemical potentials rapidly drives the magnetization to its equilibrium value. However, around the Curie temperature at 631 K [26], the chemical potentials are nearly equal and the equilibration time according to Eq. (7) reaches rather high values up to nanoseconds, thus, the magnetization dynamics is extremely decelerated. The fluences $F/F_0 \approx 2.0 - 2.4$ drive the system into this critical region, appearing red in Fig. 2. For low and very high laser fluences this region is circumvented. Thus, the μTM directly illustrates the origin of a critical slowing down and explains why experiments show a maximum in demagnetization time [12], by utilizing basic thermodynamical concepts.

In conclusion, we derived the μT model for itinerant ferromagnets. The description traces the dynamics of spin-resolved electron temperatures *and* chemical potentials simultaneously and combined with the coupling to the lattice. The demagnetization process can be described based on a few fundamental physical concepts, like dynamic exchange splitting and the relaxation towards thermodynamic equilibrium. Our method identifies the minimum of the magnetization as a transient equilibrium state of the electron systems. We explain the experimentally observed slowing down of the magnetization dynamics by a critical region in the magnetic phase diagram, Fig. 2. For certain fluences, the system is driven into this region and the time to reach the equilibrium magnetization increases considerably.

Financial support of the Deutsche Forschungsgemeinschaft through the Heisenberg project RE 1141/15 “Ultrafast Dynamics of Laser-excited Solids” is gratefully acknowledged.

* bmueller@physik.uni-kl.de

[1] T. W. McDaniel, Journal of Physics: Condensed Matter **17**, R315 (2005)
[2] E. Beaurepaire, J.-C. Merle, A. Daunois, and J.-Y. Bigot, Physical Review Letters **76**, 4250 (1996)
[3] A. J. Schellekens, W. Verhoeven, T. N. Vader, and B. Koopmans, Applied Physics Letters **102**, 252408 (2013)
[4] A. J. Schellekens and B. Koopmans, Physical Review Letters **110**, 217204 (2013)
[5] C. Illg, M. Haag, and M. Fähnle, Physical Review B **88**, 214404 (2013)
[6] K. Carva, M. Battiato, and P. M. Oppeneer, Physical Review Letters **107**, 207201 (2011)
[7] M. Battiato, K. Carva, and P. M. Oppeneer, Physical Review Letters **105**, 027203 (2010)
[8] A. Eschenlohr, M. Battiato, P. Maldonado, N. Pontius, T. Kachel, K. Holldack, R. Mitzner, A. Föhlisch, P. M. Oppeneer, and C. Stamm, Nature materials **12**, 332 (2013)
[9] E. Turgut, C. La-o vorakiat, J. M. Shaw, P. Grychtol,

H. T. Nembach, D. Rudolf, R. Adam, M. Aeschlimann, C. M. Schneider, T. J. Silva, M. M. Murnane, H. C. Kapteyn, and S. Mathias, Physical Review Letters **110**, 197201 (2013)
[10] S. Kaltenborn, Y.-H. Zhu, and H. C. Schneider, Physical Review B **85**, 235101 (2012)
[11] S. Essert and H. C. Schneider, Physical Review B **84**, 224405 (2011)
[12] B. Koopmans, G. Malinowski, F. Dalla Longa, D. Steiauf, M. Fähnle, T. Roth, M. Cinchetti, and M. Aeschlimann, Nature Materials **9**, 259 (2010)
[13] B. Y. Mueller, T. Roth, M. Cinchetti, M. Aeschlimann, and B. Rethfeld, New Journal of Physics **13**, 123010 (2011)
[14] B. Y. Mueller, A. Baral, S. Vollmar, M. Cinchetti, M. Aeschlimann, H. C. Schneider, and B. Rethfeld, Physical Review Letters **111**, 167204 (2013)
[15] M. Krauss, T. Roth, S. Alebrand, D. Steil, M. Cinchetti, M. Aeschlimann, and H. C. Schneider, Physical Review B **80**, 180407 (2009)
[16] D. Steil, S. Alebrand, T. Roth, M. Krauß, T. Kubota, M. Oogane, Y. Ando, H. C. Schneider, M. Aeschlimann, and M. Cinchetti, Physical Review Letters **105**, 217202 (2010)
[17] B. Koopmans, J. J. M. Ruigrok, F. Dalla Longa, and W. J. M. de Jonge, Physical Review Letters **95**, 267207 (2005)
[18] M. Fähnle, J. Seib, and C. Illg, Physical Review B **82**, 144405 (2010)
[19] J. Walowski, G. Müller, M. Djordjevic, M. Münzenberg, M. Kläui, C. A. F. Vaz, and J. A. C. Bland, Physical Review Letters **101**, 237401 (2008)
[20] E. Carpene, E. Mancini, C. Dallera, M. Brenna, E. Puppin, and S. De Silvestri, Physical Review B **78**, 174422 (2008)
[21] T. Roth, A. J. Schellekens, S. Alebrand, O. Schmitt, D. Steil, B. Koopmans, M. Cinchetti, and M. Aeschlimann, Physical Review X **2**, 021006 (2012)
[22] S. I. Anisimov, B. L. Kapeliovich, and T. L. Perel'man, Sov. Phys. JETP **39**, 375 (1974)
[23] W. Nolting and A. Ramakanth, *Quantum Theory of Magnetism* (Springer, Berlin Heidelberg, 2009)
[24] Z. Lin, L. V. Zhigilei, and V. Celli, Physical Review B **77**, 075133 (2008)
[25] F. Tyler, Philosophical Magazine Series 7 **11**, 596 (1931)
[26] D. R. Lide, G. Baysinger, L. I. Berger, R. N. Goldberg, H. V. Kehiaian, K. Kuchitsu, G. Rosenblatt, D. L. Roth, and D. Zwillinger, *CRC Handbook of Chemistry and Physics* (CRC Press, 2005)
[27] B. Y. Mueller and B. Rethfeld, Physical Review B **87**, 035139 (2013)
[28] O. Chubykalo-Fesenko, U. Nowak, R. W. Chantrell, and D. Garanin, Physical Review B **74**, 094436 (2006)
[29] M. G. Münzenberg, Nature Materials **9**, 184 (2010)